Saudi Journal of Biological Sciences 27 (2020) 1726–1736

Contents lists available at ScienceDirect

Saudi Journal of Biological Sciences

journal homepage: www.sciencedirect.com

Original article

Zeolitic imidazolate framework-8 (ZIF-8) doped TiZSM-5 and Mesoporous carbon for antibacterial characterization

Vijaya Ravinayagam [a,*], Suriya Rehman [b]

[a] Deanship of Scientific Research & Department of Nano-Medicine Research, Institute of Research and Medical Consultations, Imam Abdulrahman Bin Faisal University, P.O. Box 1982, Dammam 31441, Saudi Arabia
[b] Departmentof Epidemic Diseases Research, Institute of Research and Medical Consultations (IRMC), Imam Abdulrahman Bin Faisal University, P.O. Box 1982, Dammam 31441, Saudi Arabia

ARTICLE INFO

Article history:
Received 5 December 2019
Revised 6 May 2020
Accepted 7 May 2020
Available online 16 May 2020

Keywords:
Ti-ZSM-5
ZIF-8
Zinc nanoparticles
Mesoporous carbon
Antibacterial activity

ABSTRACT

Drug resistant bacteria affects millions worldwide and remains a serious threat to health care system. The study reports the first application of hybrid nanocomposites based on zeolitic imidazolate framework-8 (ZIF-8) with MFI structured zeolite Ti-ZSM-5 (TiZ5) and mesoporous carbon (MC). The composite was designated as TiZ5/ZIF-8 and MC/ZIF-8 was studied for antibacterial activity. Bioactive components Zn^{2+} and 2-methyl imidazole present in ZIF-8 was found to exert significant antibacterial effect on *Escherchia. coli* and *Staphyloccocus*. No other antibiotic drugs are required. For comparative purpose, Fe-BTC MOF (BTC = 1,3,5-benzenetricarboxylate) was used as second set of nanoformulations (TiZ5/Fe-BTC and MC/Fe-BTC) but showed a lower antibacterial activity. The phase (X-ray diffraction), texture (BET surface area), coordination (DRS-UV–Vis), and morphology (TEM) was investigated. XRD showed the presence of nanosized ZIF-8 over TiZ5 and MC. Surface area calculation using N_2 adsorption isotherm showed a reduction in the micropore surface area of ZIF-8 from 1148 m^2/g to 224 m^2/g (80%) and an increased meso surface area from 31 m^2/g to 59 m^2/g (90%). The mesopore pore volume increased significantly from 0.05 cm^3/g to 0.12 m^2/g. MC/ZIF-8 showed similar textural modifications. FT-IR spectra and DRS-UV–Vis spectra showed distinct composite formation with TiZ5, while a weak absorption of ZIF-8 observed over MC. TEM revealed the presence of nanocomposite MC/ZIF-8 and TiZ5/ZIF-8 distributed in nanosize ranging between 25 and 50 nm. TiZ5/ZIF-8 showed the minimal inhibitory concentration (MIC) and minimal bactericidal concentration (MBC) of 0.5 and 1 mg/ml, respectively against *E. coli*. The MIC and MBC of TiZ5/ZIF-8 against *S. aureus* were 1 and 2 mg/ml, respectively. MC/ZIF-8 composite had second best antibacterial activity. This study shows that ZIF-8 based composite holds a great potential against *E. coli* and *S. aureus*.

1. Introduction

Zinc metal oxide with antibacterial property is widely used in biomedical applications. The metal is biocompatible and eco-friendly. Zn^{2+} from zinc metal oxide has been reported to improve the keratinocyte movements and assist wound healing (Rath et al., 2016, Rasul Rakhshaei and Namazi, 2017). Recently, metal organic frameworks (MOFs) with structure imitating inorganic porous zeolite designated as zeolitic imidazolate frameworks (ZIF-8) has been reported. The aluminosilicate structure consist of Zn^{2+} metal ions with imidazolate linker. ZIF-8 has been applied in biomedical applications (Park et al., 2006). However, a number of ZIFs were microporous in nature, where pre-mature drug release was reported (Yan et al., 2014). In recent years, a various techniques have been applied to prepare the composite involving ZIF-8 and mesostructured materials. Such composites were most effective because it combines the advantage of micropore ZIF-8 and mesoporous materials.

Since prehistoric time, carbon black has been used as pigment and reinforcing agent in rubber products (Singh et al., 2019). In recent years, graphitized mesoporous carbon (MC) has been widely used as electrode materials for aqueous supercapacitors (Yang

* Corresponding author.
E-mail address: vrnayagam@iau.edu.sa (V. Ravinayagam).
Peer review under responsibility of King Saud University.

Production and hosting by Elsevier

https://doi.org/10.1016/j.sjbs.2020.05.016
1319-562X/

et al., 2019). MC structural features consists of graphite like features with high structural homogenity (few twists and noncyclic compounds) and less functional moities (Thangaraj and Senthil Kumar, 2012). MC exhibits high electronic flexibility, mechanical stability, thermal conductivity, and electronic mobility (Song et al., 2017). In composite formation with high surface area support system, MC has been effectively utilized in high performance components in electrochemical applications (Walcarius, 2017). Recently, multifunctional nanohybrids based on silicon and carbon has been reported with exemplary antibacterial and wound healing properties. The nanocomposite is shown to control the bacterial growth, decrease ulceration development and rejunevation wound healing (Hu et al., 2019). Polyethersulfone attached mesoporous carbon synthesized via phase inversion method has rendered antifouling and bacterial adhesion inhibition property for membrane derived filtration technology (Orooji et al., 2017). Silver doped mesoporous carbon have been reported to possess biofouling effect for the application of ultrafiltration membrane. The presence of carbon in composite induces bacterial anti-adhesion effect, while bactericidal effect on Bacillus subtilis and Escherichia coli occurs due to Ag nanoparticle (Orooji et al., 2018).

Among other nanosupports, titanium incorporated nanoporous composite were reported to interesting for antibacterial activity. In particular, silver nanoparticle at the surface of titanium containing mesoporous silica was reported to exert excellent antibacterial effect (Ionita et al., 2011). Recently, Titanium coated mesoporous silica has been shown to exhibit antibacterial effect at the dental implant surface. For instance, silver nanoparticles decorated with starch capping insertion over titanium coated nanoporous silica surface through sol–gel technique exhibited high and long term antibacterial activity against *Aggregatibacter actinomycetemcomitans* (Massa et al., 2014). The objective of this study is to develop a relatively simple and inexpensive antibacterial bioactive nanocomposites that can be used directly for dental implant, bone and drug delivery applications. To the best of our knowledge, a hybrid system involving graphitized mesoporous carbon (MC)/ZIF-8, and TiZ5/ZIF-8 has not been reported elsewhere. ZIF-8 containing Zn^{2+} and imidazole linker has been reported to exhibit antibacterial effect for the first time. A simple ultrasonic technique have been applied to prepare the composite involving ZIF-8 with MC and TiZ5. Such composites can be easily upgraded for ultrafiltration membrane derived filteration technology and dental implant.

2. Materials and methods

ZIF-8 (Basolite Z1200) with surface area of 1040 m^2/g were purchased from Sigma Aldrich. Fe-BTC (Basolite F-300) was purchased from BASF. The MOF exhibited a high surface area of 1300–1600 m^2/g. Graphitized mesoporous carbon with surface area of 50–100 m^2/g with pore volume of 0.25 cm^3/g was obtained from Sigma-Aldrich.

2.1. Preparation of TiZSM-5 (TiZ5)

TiZ5 was prepared by dissolving 11.42 g of ludox AS-40 with 0.63 ml of TIP (Si/Ti ratio 10) and Aluminium nitrate (Si/Al ratio 25). The ratio of F/Si = 1.0 was maintained in synthesis solution. Then 8 g of TPAOH (40%) was added dropwise and stirred for 1 h. 0.93 g of NaOH dissolved in 9 ml water was then added dropwise and stirred overnight. Then solution aged and kept in static oven hydrothermally treated at 160 °C for 72 h, filtered, dried and calcined at 550 °C for 6 h at 5 °C/min.

2.2. Preparation of TiZSM-5/ZIF-8 (TiZ5/ZIF-8)

2.4 g of TiZSM-5 and 252 mg of ZIF-8 was dissolved in methanol (300 ml) and sonicated for 10 min. The composite TiZ5/ZIF-8 was recovered through centrifugation. Similar procedure was followed to prepare the sample TiZ5/Fe-BTC, where Fe-BTC used instead of ZIF-8.

2.3. Preparation of Mesoporous carbon/ZIF-8 (MC/ZIF-8)

2.4 g of MC and ZIF-8 (252 mg) was dissolved in methanol (300 ml) and stirred for dissolution, then sonicated for 10 min. Then the solution composite was centrifuged and collected. The loaded formulations was labelled as, MC/ZIF-8 (Table 1). Similar procedure was followed to prepare the sample MC/Fe-BTC, where Fe-BTC used instead of ZIF-8.

2.4. Nanomaterial characterization

The phase analysis of nanocomposites TiZ5/ZIF-8, TiZ5/Fe-BTC, MC/ZIF-8 and MC/Fe-BTC was analyzed using benchtop Rigaku Multiplex system, Japan. Surface area and pore size distributions was measured using N_2 and Argon adsorption isotherm using ASAP-2020 plus (Micromeritics, USA). The functional groups of ZIF-8, F300 and TiZ5 functional groups were observed by FT-IR spectroscopy (Perkin Elmer, USA). The morphological structure of composite was measured using TEM analysis (JEM2100F from JEOL). The coordination nature of metal ion species were determined using diffuse reflectance spectroscopy (JASCO, Japan).

2.5. Study of antibacterial activity of nanocomposites

Gram-negative bacteria, *Escherchia. coli ATCC35218* and Gram-positive, *Staphyloccocus. aureus ATCC29213*, were chosen for the antibacterial activity of synthesized nanocomposites i.e., TiZ5/Fe-BTC, TiZ5/ZIF-8, MC/Fe-BTC and MC/ZIF-8. Briefly, overnight incubation *of E. coli* and *S. aureus* was done in a nutrient broth (NB) using an incubator shaker (150 rpm) at 37 °C. The cell pellets were obtained and washed using phosphate buffer (PBS) to get rid of the residual media. *E. coli* and *S. aureus* cell suspensions were adjusted to the cell density of approximately 10^7 CFU/ml by diluting with sterile 0.9% NaCl solution.

Minimal inhibitory concentration (MIC): The experiment was carried on Mueller Hinton Agar (MHA) plates. The antibacterial activities of TiZ5/Fe-BTC, TiZ5/ZIF-8, MC/Fe-BTC and MC/ZIF-8 nanocomposites were examined as per the method previously described by Rehman et al., (2019). The MIC was obtained by dilutions of synthesized NPs in the concentrations ranging from 8 mg/ml to 0.25 mg/ml. The MIC was taken as the minimum concentration of test nanocomposites, which appeared with no visual growth.

Minimal bactericidal concentration (MBC). The nanocomposites were further subjected to MBC assessment. Briefly, 10 μl of overnight grown culture, i.e., treated and untreated (control) *E.coli* and *S.aureus* were transferred by streaking onto the fresh MHA plates and reincubated for overnight at 37 °C. After the observation, the MBC was taken as the minimum concentration of nanoparticles, which appeared with no growth of bacteria or with less than three CFUs (Rehman et al., 2019).

2.6. Study of morphogenesis using SEM

The effect of TiZ5/Fe-BTC, TiZ5/ZIF-8, MC/Fe-BTC and MC/ZIF-8 nanocomposites on the topology of treated and untreated bacteria was further studied by SEM. Precisely, adjusted cell density of bacterial cells were incubated with obtained sub-MIC values (Figs. 3

Table 1
Physico-chemical analysis ZIF-8, Fe-BTC, TiZ5 and Mesoporous carbon composites.

Sample	SA_{BET} (m^2/g)	MSA (m^2/g)	MesoSA (m^2/g)	TPV (cm^3/g)	MicroPV (cm^3/g)	MesoPV (cm^3/g)	APD (nm)
ZIF-8	1148	1117	31	0.67	0.62	0.05	2.3
TiZ5/Fe-BTC	426	275	151	0.40	0.16	0.24	3.8
TiZ5/ZIF-8	224	165	59	0.21	0.09	0.12	3.8
MC/Fe-BTC	133	46	87	0.41	0.02	0.39	12.5
MC/ZIF-8	188	110	78	0.46	0.06	0.40	10.2

SA_{BET} = BET Surface area, MSA = Micropore surface area, MesoSA = Mesoporous surface area, PV = Total pore volume, MicroPV = micropore volume, MesoPV = mesopore pore volume, APD = Average pore diameter.

and 4) of TiZ5/Fe-BTC, TiZ5/ZIF-8, MC/Fe-BTC and MC/ZIF-8 nanocomposites at 37 °C. The untreated and treated cell pellets were obtained by centrifugation at 12,000 rpm and washed several times with PBS. Later cells were subjected to primary fixation using 2.5% glutaraldehyde, followed by treatment with 1% osmium tetroxide as a secondary fixative. Fixed cell samples were washed and then dehydrated by varying concentration of ethanol i.e., 35%, 55%, 75%, 95% and 100%. The dehydrated cell was placed on the aluminum stubs, and dried using a desecrator. The dried samples were coated with gold and finally examined at an accelerating voltage of 20 kV by SEM (Mohammad et al., 2018).

3. Results and discussion

Fig. 1 shows the X-ray diffraction pattern of ZIF-8, Fe-BTC, MC, MC/ZIF-8, MC/Fe-BTC, TiZ5/ZIF-8, TiZ5/Fe-BTC and TiZ5. ZIF-8 showed characteristics diffractions in line with earlier reports (Du et al., 2016). MC showed a broad peak at 2θ value of about 25.9° corresponding to the amorphous characteristics of mesoporous carbon. MC/ZIF-8 showed the presence of similar broad reflection to that of MC but with additional peaks of ZIF-8. However, the reduced intensity of ZIF-8 demonstrates a partial transformation of crystalline ZIF-8 to nanosize at the pores of MC, while preserving the ZIF-8 structure. In case of Fe-BTC, the crystalline peaks of parent MOFs was clearly not seen in the composite, which indicates the complete crystalline transformation. Fe-BTC showed a weak diffraction peaks corresponding to amorphous iron coordinated sites. In case of MC/Fe-BTC composite, a less intense broad peak at 10.5° showed transformation of amorphous Fe-BTC. TiZ5 showed characteristics peaks of MFI structured ZSM-5. ZIF-8 transformation to nanosize is more pronounced in ZSM-5 than MC. It clearly shows the advantage of MFI structure with zigzag pores (0.51 nm). Fe-BTC peaks were not observed and showed the complete nanotransformation.

The textural nature of ZIF-8, Fe-BTC, MC/ZIF-8, MC/Fe-BTC, TiZ5/ZIF-8 and TiZ5/Fe-BTC was analyzed by nitrogen adsorption isotherm (Fig. 2). Parent ZIF-8 showed a steep increase in nitrogen uptake at lower p/p0 indicating high ratio of micropores with BET surface area of 1148 m^2/g (Liu et al., 2017). The composites MC/ZIF-8, MC/Fe-BTC, TiZ5/ZIF-8 and TiZ5/Fe-BTC exhibited a typical Type 1 isotherms characteristics of micropores with BET surface area of 188 m^2/g, 133 m^2/g, 224 m^2/g and 426 m^2/g. TiZ5/ZIF-8 and TiZ5/Fe-BTC showed a slight increase in hysteresis at higher p/p0 ratio indicating presence of few mesopores along with micropores. The nitrogen adsorption over TiZ5/ZIF-8 and TiZ5/Fe-BTC showed the mesoporous surface area of 59 m^2/g and 151 m^2/g.

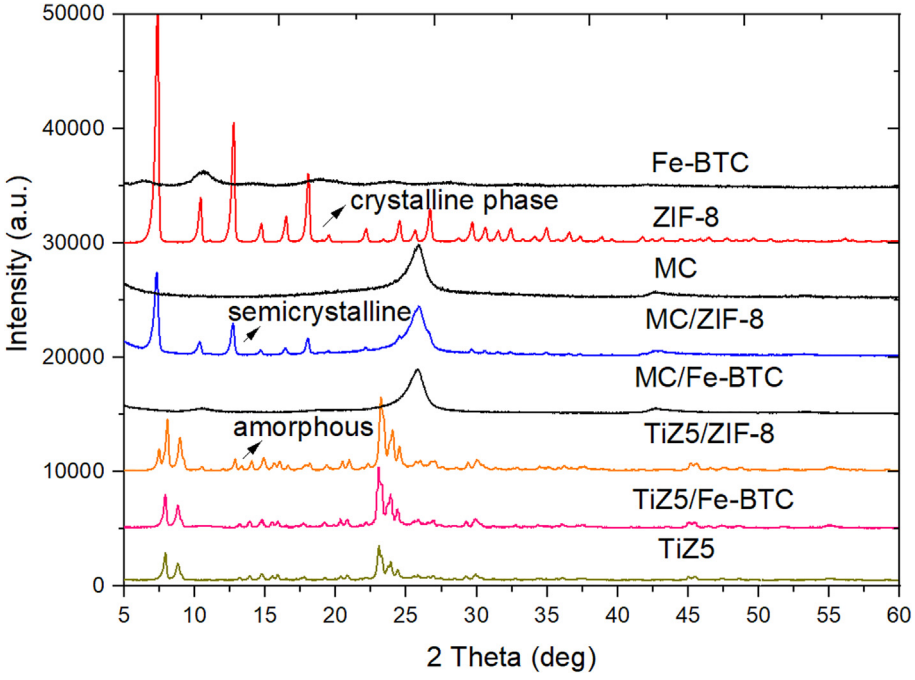

Fig. 1. X-ray diffraction pattern of ZIF-8, Fe-BTC, MC, MC/ZIF-8, MC/Fe-BTC, TiZ5/ZIF-8, TiZ5/Fe-BTC and TiZ5.

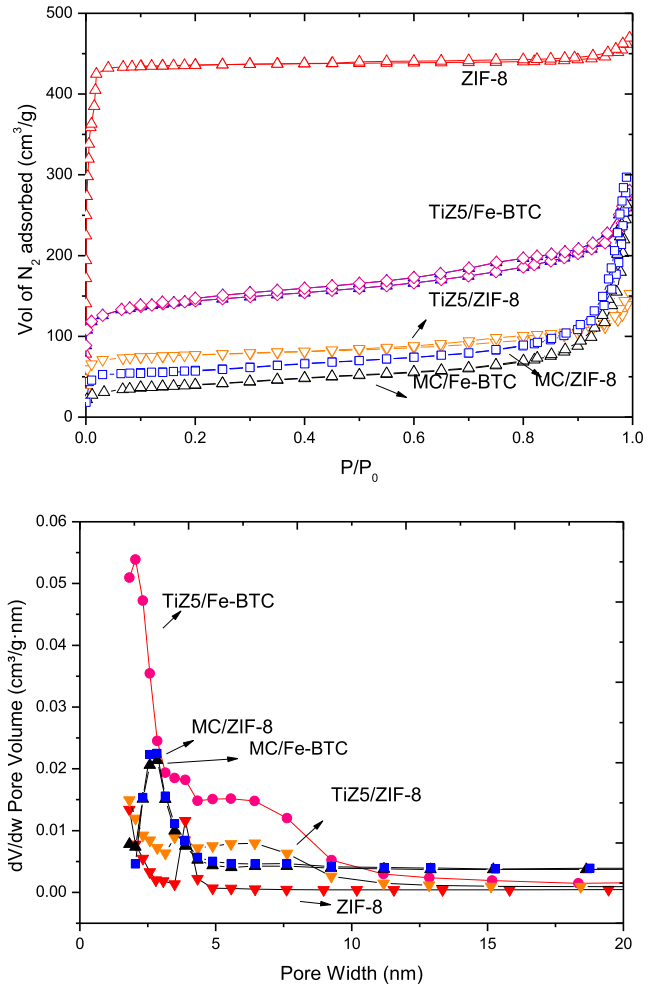

Fig. 2. Nitrogen adsorption isotherm and pore size distributions of ZIF-8, Fe-BTC, MC/ZIF-8, MC/Fe-BTC, TiZ5/ZIF-8 and TiZ5/Fe-BTC.

The pore size distribution also replicates the isotherm pattern with a broad pore size distribution over TiZ5/ZIF-8 and TiZ5/Fe-BTC. In case of composite with mesoporous carbon, MC/ZIF-8 and MC/Fe-BTC showed a uniform pore size distribution centered at average pore diameter of 10.2 and 12.5 nm. Pore volume of TiZ5/Fe-BTC composite was higher than that of TiZ5/ZIF-8. MC/ZIF-8 and MC/Fe-BTC showed similar pore volume of about 0.41 and 0.46 cm^3/g. Moreover, TiZ5 or MC tends to safeguard the structural configuration of MOFs. ZIF-8 containing micropores showed a steep micropore filling at lower p/p0. The BET surface area was 1148 m^2/g. The t-plot represented the presence of high micropore surface area of 1117 m^2/g and less mesopore surface area of 31 m^2/g over ZIF-8. In case of TiZ5/Fe-BTC and TiZ5/ZIF-8, the micropore reduces and remains at 275 m^2g and 165 m^2g. High mesosurface area of 151 m^2g was observed over TiZ5/Fe-BTC, while it reduces to 59 m^2g with TiZ5/ZIF-8. In case of mesoporous carbon, MC/Fe-BTC composite have BET surface area of 133 m^2/g, in which 46 m^2/g tends to be of mesopore surface area. The BET surface area and MSA of MC/ZIF-8 is found to be high of 188 m^2/g and 110 m^2/g. The mesopore volume tends to increase significantly with composite formation. Active formulations, TiZ5/ZIF-8 and MC/ZIF-8 pore volume were increased to 0.12 cm^3/g and 0.40 cm^3/g. In case of TiZ5, the average pore diameter increases from 2.3 nm to 3.8 nm, while MC/Fe-BTC and MC/ZIF-8 showed highest pore diameter of 12.5 nm and 10.2 nm.

Fig. 3 shows the functional groups of ZIF-8 and TiZ5/ZIF-8. ZIF-8 presented a sharp vibration bands between 1395 and 1468, 1382, 1311, 1182, 1150, 995, 954, 760, 692 and 685 cm^{-1} consistence with earlier reports (Ordonez et al., 2010, Zhang et al., 2018). In case of TiZ5/ZIF-8, a small but distinct peaks of ZIF-8 correspondings to C = N and C-N appeared at 1582 cm^{-1}, 1147 cm^{-1} and 958 cm^{-1}. The signals of aromatic imidazole ring was found to appear between 1308 and 1455 cm^{-1}. Importantly, the presence of distinct Ti-O-Si stretching vibration was observed at 800 cm^{-1}, indicating the chemical interaction of TiZSM-5 with ZIF-8. In case of MC/ZIF-8, a distinct signals indicating a functional interactions between MC and ZIF-8 was not observed in the FTIR characterization tool, which can be attributed due to symmetric nature of MC. However, the interaction has been confirmed using XRD (Fig. 1) and the subsequent study using DRS-UV spectroscopy and TEM analysis (Figs. 4 and 6).

Fig. 4 shows the spectra of DRS-UV–vis spectra of MC/ZIF-8, MC/Fe-BTC, TiZ5/ZIF-8 and TiZ5/Fe-BTC. ZIF-8 has been reported to exhibit a absorption peak at 230 nm due to Zn^{2+} species of ZIF-8 (Huang et al., 2018). With composite formation with TiZ5, an expansion in the absorption peak due to TiO_2 occurs at about 300 nm. Basolite F300 composite with TiZ5 showed the absorption expanding to the visible region till 700 nm. MC/ZIF-8 and MC/Fe-BTC showed only a weak absorption peak corresponding to ZIF-8 and Fe-BTC.

The morphological features of TiZ5/ZIF-8 and MC/ZIF-8 were analyzed using transmission electron microscope (Fig. 5). The presence of ZIF-8 as composite was observed with TiZ5. ZIF-8 with nanosize ranging between 25 and 50 nm was found to coexist with TiZ5 zeolite to form TiZ5/ZIF-8 composite. The size of ZIF-8 was reduced slightly corresponding to the typical range of ZIF-8 crystals (40–70 nm) without TiZ5 (Liu et al., 2017). The TiO_2 and Zn nanoparticles with dspacing of 0.25 nm and 0.22 nm was microscopically captured showing coexisting over ZSM-5 support (Fig. 5). The textural characteristics of MC/ZIF-8 showed the nanotextures of MC in pentagonal structure with diameter ranging about 35 nm. The MC nanoparticles can be clearly seen in agglomerated form in size range of 175 nm. Unlike TiZ5, the presence of ZIF-8 was not clearly distinguishable that might be due to thickness of MC (Fig. 6).

3.1. Study of antibacterial activity of nanocomposites against E. coli and S. aureus

The antibacterial activity of TiZ5/Fe-BTC, TiZ5/ZIF-8, MC/Fe-BTC and MC/ZIF-8 nanoparticles in this study has been reported for the first time to the best of our knowledge. Although carbon-based nanoparticles like carbon nanotubes and graphene oxide has been previously reported by various research groups (Sui et al., 2013; El-Shafai et al., 2019). In the current study, synthesized nanocomposites were subjected to antibacterial activities against *E. coli* and *S. aureus* by evaluating the MIC and MBCs values.

The MIC and MBC for TiZ5/Fe-BTC nanocomposite were 1 and 4 mg/ml, respectively, whereas TiZ5/ZIF-8 showed the MIC and MBC of 0.5 and 1 mg/ml, respectively against *E. coli* (Fig. 7a&b). The recorded MIC and MBC values for MC/Fe-BTC were found as >8 mg/ml and MC/ZIF-8 was 1 and 2 mg/ml, respectively Fig. 7a&b). It has been observed that the TiZ5/ZIF-8 and MC/ZIF-8 nanocomposite depicted significant activity as compared to the TiZ5/Fe-BTC and MC/Fe-BTC.

The MIC and MBC for TiZ5/Fe-BTC nanoparticles were 8 and >8 mg/ml, respectively, whereas TiZ5/ZIF-8 showed the MIC and MBC of 1 and 2 mg/ml, respectively against *S. aureus* (Fig. 8). The MICs and MBCs values for MC/Fe-BTC were found >8 mg/ml

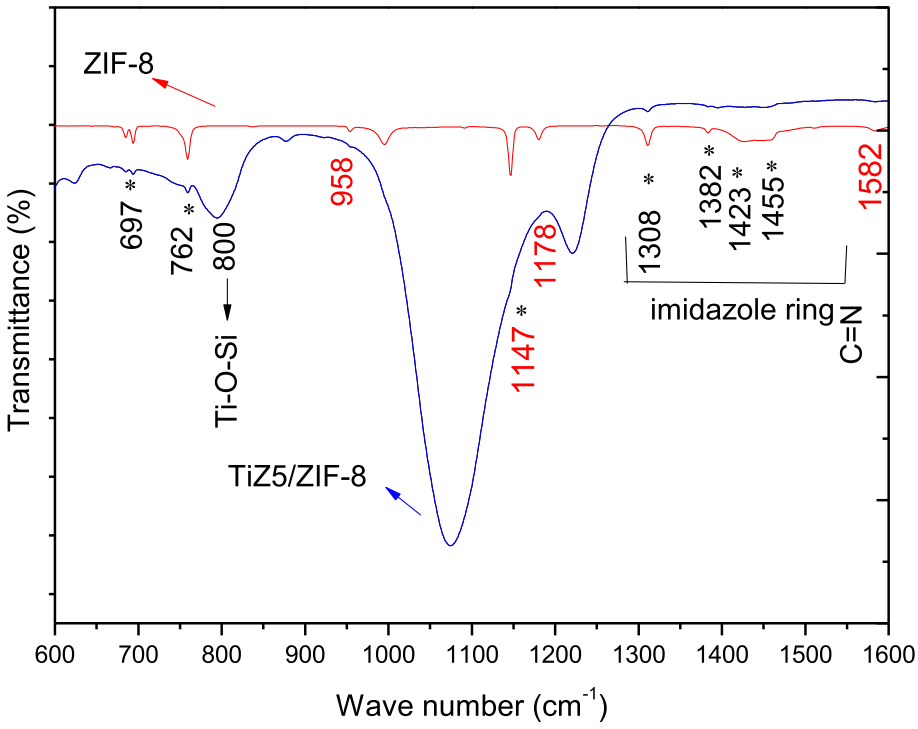

Fig. 3. FTIR spectra of ZIF-8 and TiZ5/ZIF-8.

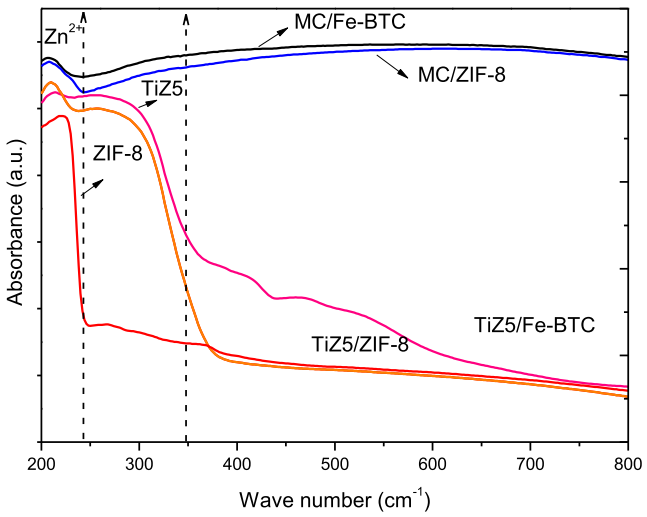

Fig. 4. DRS-UV spectra of MC/ZIF-8, MC/Fe-BTC, TiZ5/ZIF-8 and TiZ5/Fe-BTC.

and MC/ZIF-8 nanocomposite was 1 and 4 mg/ml, respectively. Therefore, it has been observed that the TiZ5/ZIF-8 and MC/ZIF-8 nanocomposite depicted significant activity as compared to the TiZ5/Fe-BTC and MC/Fe-BTC against *S. aureus* as well.

3.2. Study of morphogenesis using SEM

The topology changes of *E. coli* and *S. aureus*, caused by TiZ5/Fe-BTC, TiZ5/ZIF-8, MC/Fe-BTC and MC/ZIF-8 nanocomposites were also studied by SEM. The control *E. coli* cells (untreated cells) were appearing as rod-shaped with consistent cell surface (Fig. 9a). The *E. coli* treated with TiZ5/Fe-BTC showed a moderately damaged cells (Fig. 9b), although, when treated with TiZ5/ZIF-8, the count of *E. coli* cells showed a reduction in number and were significantly damaged with distorted cell wall and membrane (Fig. 9c). This damage caused a loss of integrity of cell wall and membrane, leading to death of bacteria. Similarly, treatment of *E. coli* with MC/Fe-BTC did not show any significant change in the structure and number of cells (Fig. 9d), whereas treatment with MC/ZIF-8 nanocomposite depicted the distortion and deformation of cells with reduced cell count (see Fig. 9e).

On the other hand, the control cells of *S. aureus* cells (untreated) were normal in shape, depicting the smooth cell surface (Fig. 10a). The treatment with TiZ5/Fe-BTC have had almost no apparent effect on the structure of *S. aureus* cells (Fig. 10b), however, when treated with TiZ5/ZIF-8, the S. aureus cells appeared as reduced in number and were effectively damaged. The cells were found to have lost the integrity due to the damage and deformation of cellular wall and membrane which ultimately leads to cell death (Fig. 10c). Similar picture of topological changes was found in S. *aureus* cells, when treated with MC/Fe-BTC and MC/ZIF-8 (Fig. 10d&e).

Zinc oxide is a proven antibacterial element against numerous microorganisms (Vimbela et al., 2017). The nanostructure of ZnO with respect to size and shape depends on the synthesis protocols such as residence time and temperatures (Emil et al., 2018). Hu et al. (2009) reported that the effect of metal oxide over bacteria depends on the nanoparticle shape, size, concentration and time of exposure. The shape of ZnO reported so far includes nanorods, nanotubes, nanocages, nanoflower and nanoboxes (Siddiqi et al., 2018). The morphological analysis using SEM and TEM techniques showed that ZnO nanoparticle affects the cell wall of bacterial at first stage, penetrates and assemble at the cell membrane. Followingly interrupts the metabolic functions of bacteria and induces cell death (Yusof, et al., 2019). Specifically, ZnO nanoparticle was reported to induce oxidative stress and damages lipids through lipid peroxidation. Similarly, alters the proteins, DNA and carbohydrates (Sirelkhatim et al., 2015). The toxic nature of metal oxide

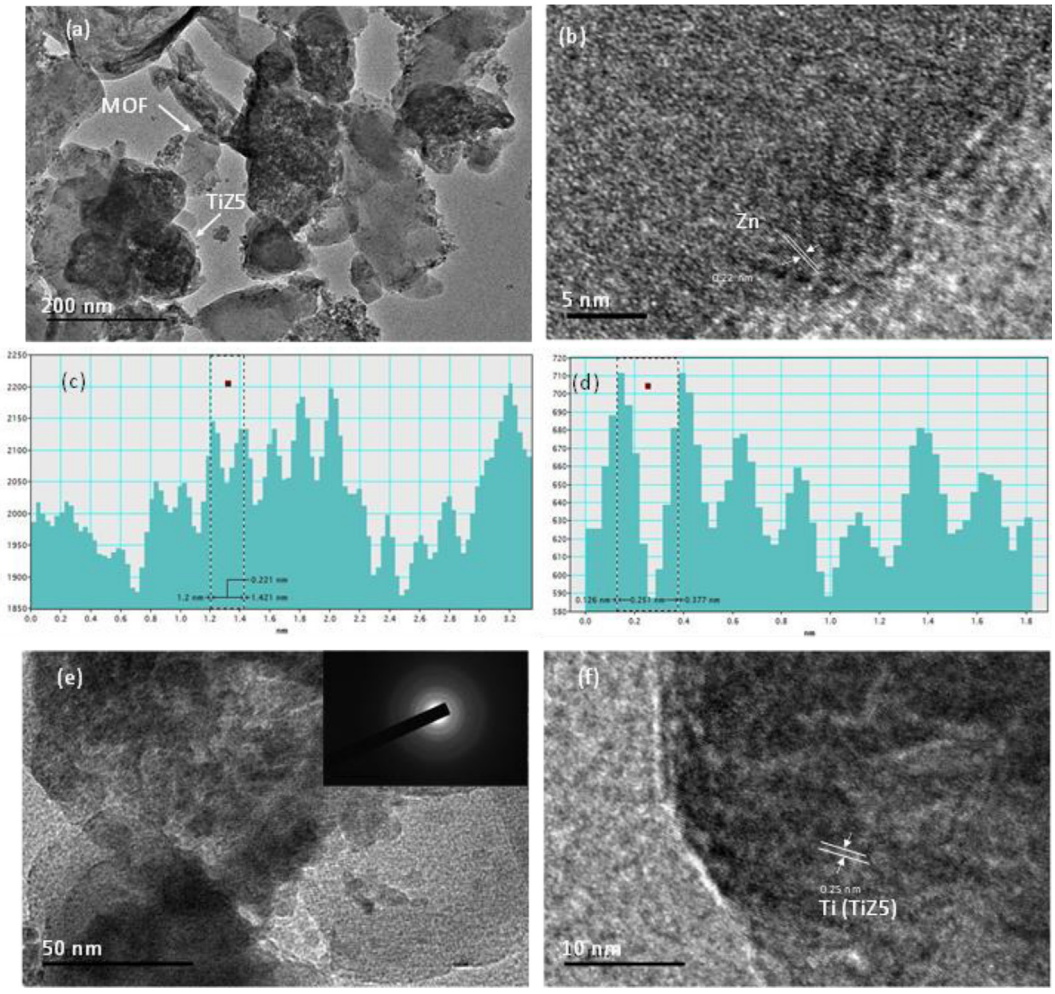

Fig. 5. TEM images **of TiZ5/ZIF-8.**

nanoparticle is primarily attributed to the release of Zn^{2+} ions that occurs by the reaction of ZnO with acids and alkalis (Sawai et al., 1998). Karlsson et al., (2014) have reported that Zn^{2+} ions were released due to extracellular dissolution of ZnO. Higher antibacterial activity of $ZnSO_4$ has been directly proportional to Zn^{2+} ions (Yung et al., 2017). It has been reported that positive charge of Zn^{2+} effectively bind with negative charge of biomolecules present inside the bacterial cell (Cho et al., 2011). A trace quantity of Zn ions is found to be effective against viruses due to higher solubility of such Zn^{2+} ions compared to zinc oxide (Rudramurthy et al., 2016).

There are numerous reports on the Zeolitic imidazole framework nanocomposites being utilized for various physical and chemical property like adsorption performance (Ma et al., 2018), pH-dependent drug delivery vehicles (Ren et al., 2014), fast gas chromatographic separation of small molecules (Yusuf et al., 2015), photocatalytic application (Pattengale et al., 2017) etc. However, the antimicrobial efficacy of such nanocomposites is yet to be studied and explored. In a report by Wang and his team studied the zeolitic imidazolate framework/graphene oxide hybrid nanosheets which were functionalized on a membrane for its antimicrobial activity (Wang et al., 2016). Although, the actual mode of action of TiZSM-5/ZIF-8 is still not studied, however, various factors can influence the obtained activity. Mainly the effect is owing to the particle characteristics, arrangement and size of subunits, stability and behavior to the specific experimental cell. It is presumed that the probable mechanism of ZIF activity obtained as TiZ5/ZIF-8 and MC/ZIF-8 due to DNA damage in the cells. However, among the series of MOF that Fe based Fe-BTC are less effective then Zn based framework. Studies on Zn nanoparticles have suggested the release of Zn ions which interferes with Zn homeostatsis and therefore resulting in mitochondrial dysfunction, enhanced release of cellular ROS and cell disintegration (Kao et al., 2011, Rehman et al., 2019).

In the current study, it has been observed that the attachment and penetration of synthesized material to microbial cell surface has a paramount importance in obtaining antibacterial activity. The penetration of material into the cell leads to the alteration in the cell wall and membrane integrity by structure recombination, loss of membrane proteins, intracellular uptake, etc. This restructuring leads to various types of interactions with ROS, antioxidant, sorbate, oxidoreductases, leading to dysregulation of cellular redox equilibrium, to combat the bacterial survival (Wang et al., 2019).

ZIF-8 containing two nanocomposites TiZ5/ZIF-8 and MC/ZIF-8 showed excellent antibacterial activity. Comparatively, Fe-BTC based two nanocomposites TiZ5/Fe-BTC and MC/Fe-BTC showed a lower antibacterial activity (Figs. 1–4). This clearly shows the antibacterial activity of ZIF-8 in composite formation with TiZ5 and MC support. TiZ5 and MC support helps to transform the crystalline ZIF-8 to semi-crystalline state and increase the solubility of

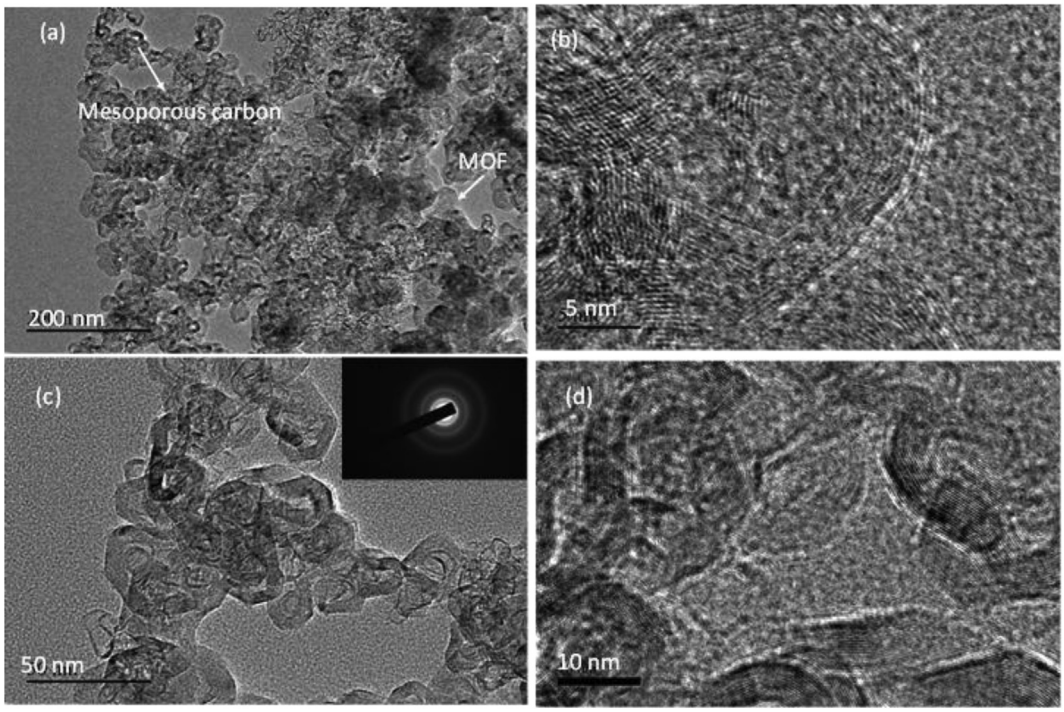

Fig. 6. TEM images of MC/**ZIF-8.**

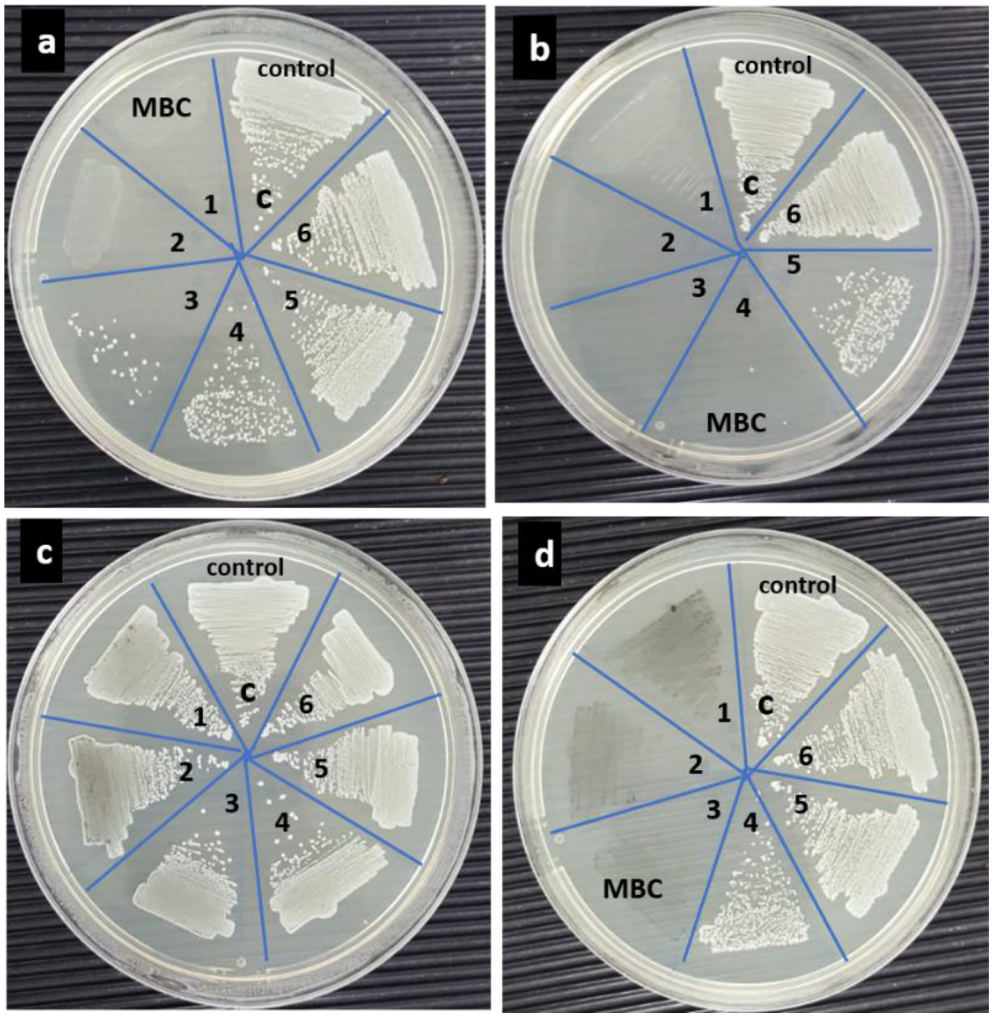

Fig. 7. MBC values of synthesized nanoparticles against *E. coli* (a) TiZ5/Fe-BTC (b) TiZ5/ZIF-8 (c) MC/Fe-BTC (d) MC/ZIF-8. (1) 8 mg/ml, (2) 4 mg/ml, (3) 2 mg/ml, (4) 1 mg/ml, (5) 0.5 mg/ml, (6) 0.25 mg/ml, (c) control without any treatment.

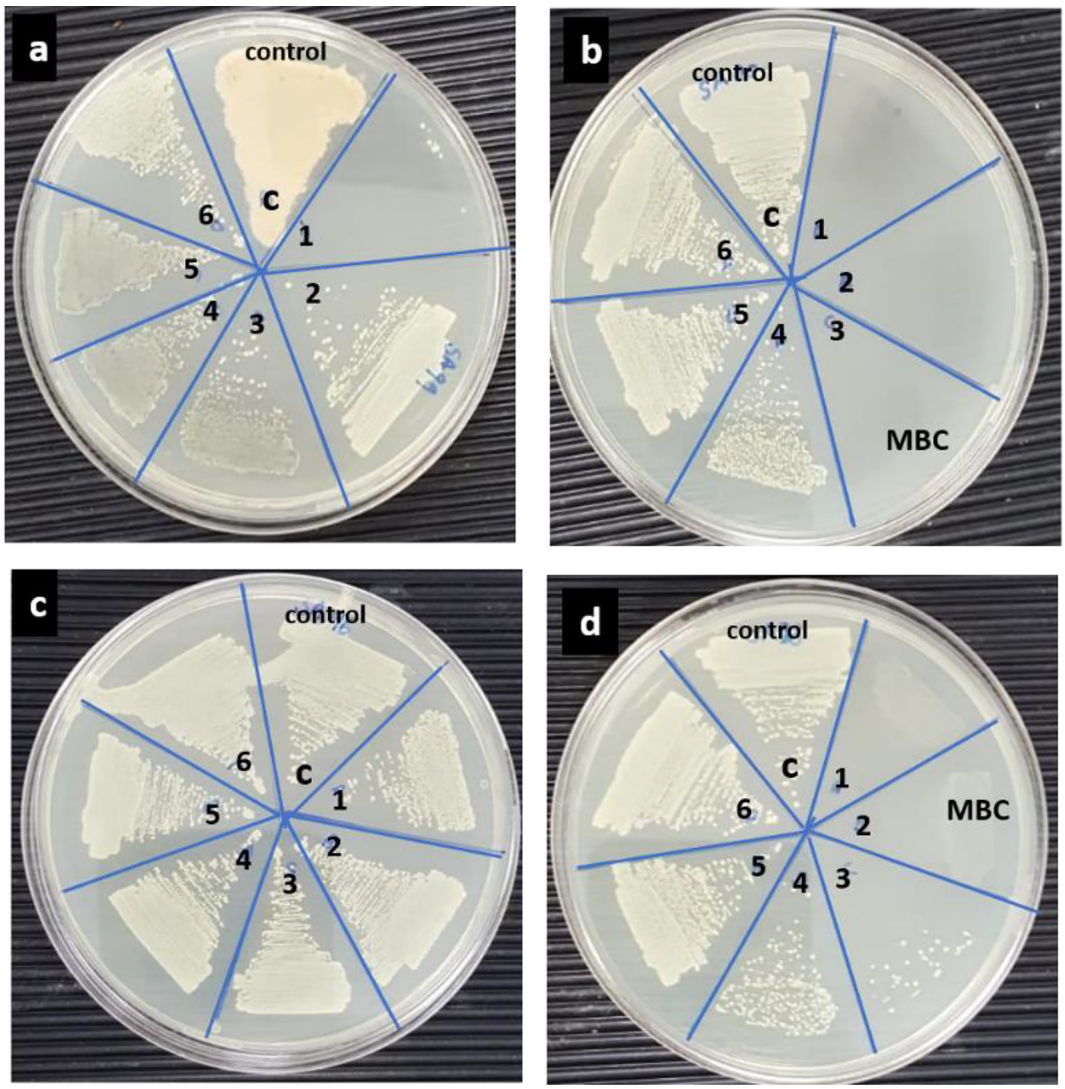

Fig. 8. MBC values of synthesized nanoparticles against *S. aureus* (a) TiZ5/Fe-BTC (b) TiZ5/ZIF-8 (c) MC/Fe-BTC (d) MC/ZIF-8. (1) 8 mg/ml, (2) 4 mg/ml, (3) 2 mg/ml, (4) 1 mg/ml, (5) 0.5 mg/ml, (6) 0.25 mg/ml, (c) control without any treatment.

ZIF-8 (Fig. 1, XRD). In ZIF-8/CNT nanocomposite, crystal size of ZIF-8 depends on the nucleation sites of carbon nanotube support. A strong interaction between imidazole linker and carbon support increases the crystal nucleation site and decrease the crystal size of ZIF-8 (Fu et al., 2018). The semi-crystalline transformation clearly shows increased interactions between imidazole and MC surface (Fig. 1, Fig. 4 and Fig. 6). ZIF-8 is know to be built with metal ions (Zn^{2+}) and imidazolate linker (Park et al., 2006). The presence of composite helps to reduce to size of Zn^{2+} and high antibacterial activity shows the increased penetration of nano sized Zn^{2+} of ZIF-8 into the cell wall leading to cell death (Scheme 1).

4. Conclusion

The study shows that antibacterial property of ZIF-8 in composite formation with TiZ5 and MC. TiZ5 with Si/Al ratio of 25 and Si/Ti ratio of 10 was synthesized in fluoride media using sol–gel technique. Transformation of crystalline to nanosized ZIF-8 over TiZ5 showed best antibacterial activity followed by mesoporous carbon MC. The isotherm pattern of TiZ5/ZIF-8 and MC/ZIF-8 showed a reduction in micropore surface area and formation of mesopores and mesopore volume indicating effective composite transition of ZIF-8. The average pore diameter showed a similar expansion in pores compared to parent supports TiZ5 and MC. Zn^{2+} present in ZIF-8 was found to exert significant antibacterial effect on Escherchia. coli and Staphyloccocus. aureus. TiZ5/ZIF-8 and MC/ZIF-8 showed a concentation dependent antibacterial effect, while Fe-BTC showed no such activity in composite with TiZ5 and MC. Overall, ZIF-8 can be a potential antibacterial component that can be further manipulated with biocompatible polymers, natural antioxidants and anticancer drugs. The simple and cost-effective nanocomposite can be easily upgraded for ultrafiltration membrane derived filteration technology and dental implant device.

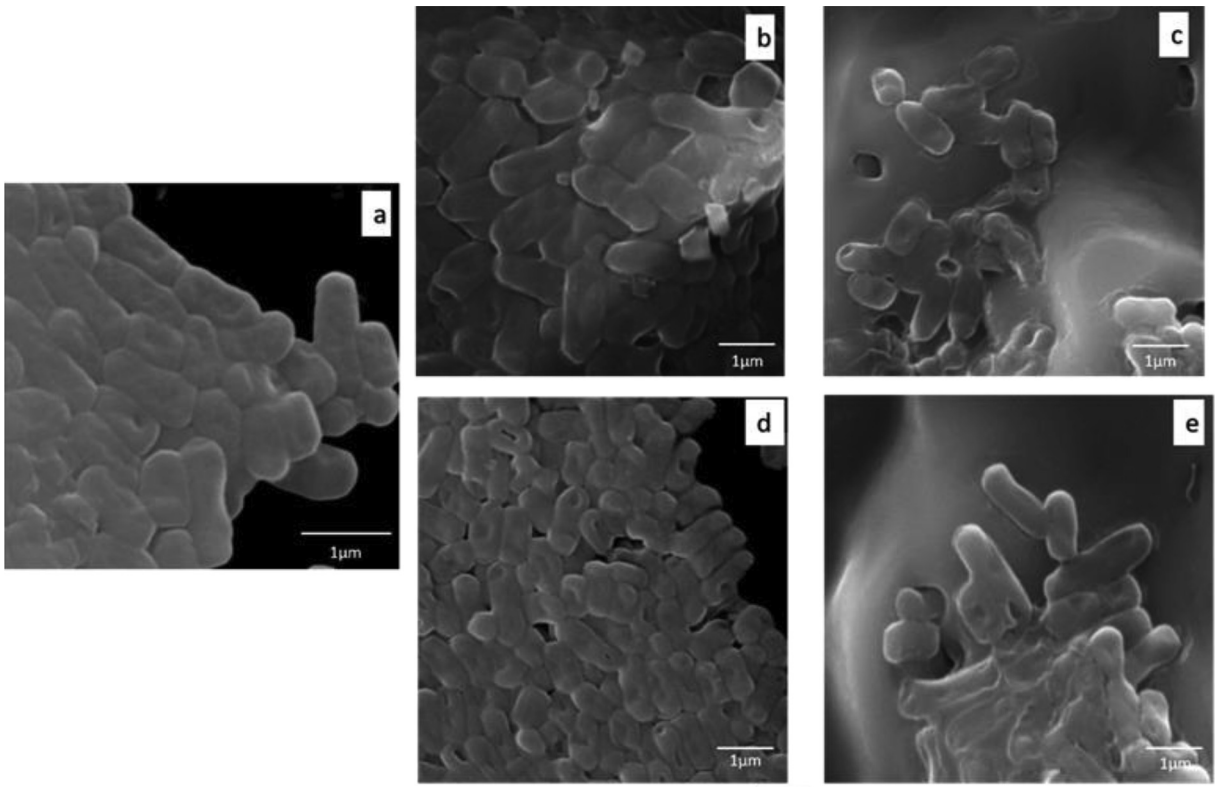

Fig. 9. SEM images for effects of synthesized nanoparticles against *E. coli* (a) Control (untreated *E. coli*) (b) TiZ5/Fe-BTC (2 mg/ml) (c) TiZ5/ZIF-8 (0.5 mg/ml) (d) MC/Fe-BTC (8 mg/ml) (d) MC/ZIF-8 (1 mg/ml).

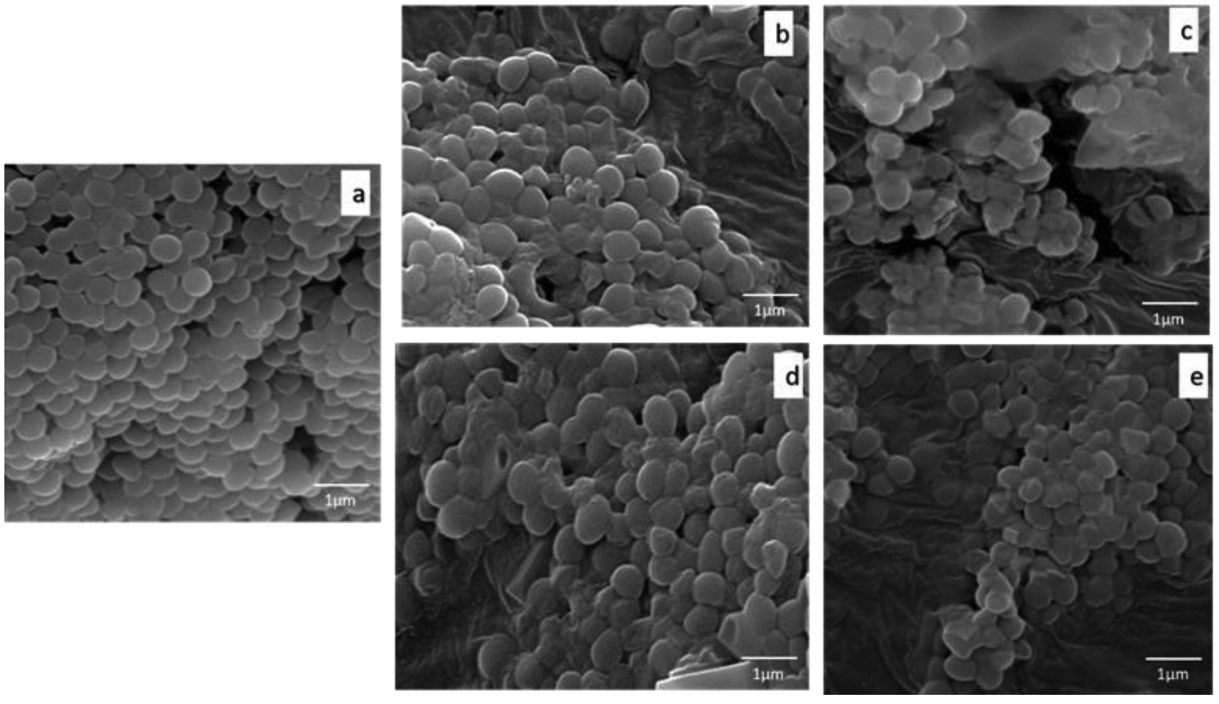

Fig. 10. SEM images for effects of synthesized nanoparticles against *S.aureus* (a) Control (untreated *S.aureus*) (b) TiZ5/Fe-BTC (2 mg/ml) (c) TiZ5/ZIF-8 (0.5 mg/ml) (d) MC/Fe-BTC (8 mg/ml) (d) MC/ZIF-8 (1 mg/ml) .

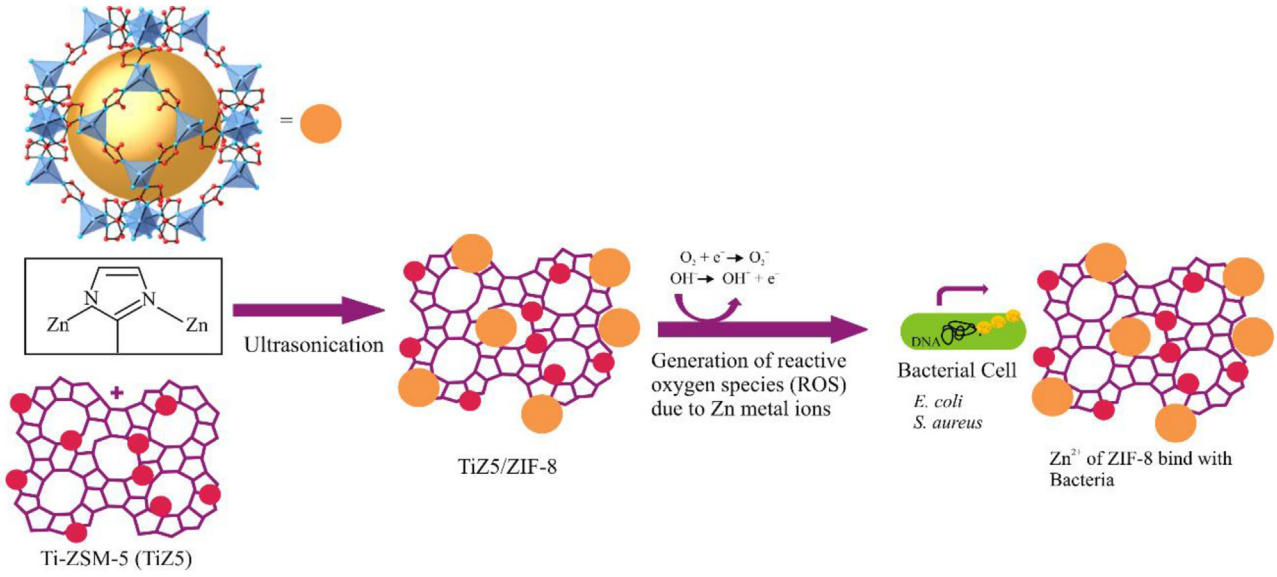

Scheme 1. Preparation of TiZSM-5/ZIF-8 nanocomposite for antibacterial activity against *E. coli* and *S. aureus*.

Declaration of Competing Interest

The authors declare that they have no known competing financial interests or personal relationships that could have appeared to influence the work reported in this paper.

Acknowledgement

Vijaya Ravinayagam acknowledge the funding obtained from Deanship of Scientific Research (DSR), IAU with grant number 2019-120-DSR. The author also thank Dr. Rabindran Jermy for providing the nanomaterials. The authors acknowledge Institute of Research and Medical Consultations for providing the research facilities.

References

Cho, W.S., Duffin, R., Howie, S.E., Scotton, C.J., Wallace, W.A., Macnee, W., Bradley, M., Megson, I.L., Donaldson, K., 2011. Progressive severe lung injury by zinc oxide nanoparticles; the role of Zn^{2+} dissolution inside lysosomes. Part. Fibre Toxicol. 8, 27. https://doi.org/10.1186/1743-8977-8-27.

Du, M., Li, L., Li, M., Si, R., 2016. Adsorption mechanism on metal organic frameworks of Cu-BTC, Fe-BTC and ZIF-8 for CO_2 capture investigated by X-ray absorption fine structure. RSC Adv. 6, 62705–62716. https://doi.org/10.1039/C6RA07582G.

El-Shafai, N., El-Khouly, M.E., El-Kemary, M., Ramadan, M., Eldesoukey, I., Masoud, M., 2019. Graphene oxide decorated with zinc oxide nanoflower, silver and titanium dioxide nanoparticles: fabrication, characterization, DNA interaction, and antibacterial activity. RSC Adv. 9, 3704–3714. https://doi.org/10.1039/C8RA09788G.

Emil, E., Alkan, G., Gurmen, S., Rudolf, R., Jenko, D., Friedrich, B., 2018. Tuning the Morphology of ZnO Nanostructures with the Ultrasonic Spray Pyrolysis Process. Metals 8, 569. https://doi.org/10.3390/met8080569.

Fu, F., Zheng, B., Xie, L.-H., Du, H., Du, S., Dong, Z., 2018. Size-Controllable Synthesis of Zeolitic Imidazolate Framework/Carbon Nanotube Composites. Crystals 8 (367). https://doi.org/10.3390/cryst8100367.

Hu, X., Cook, S., Wang, P., Hwang, H.M., 2009. In vitro evaluation of cytotoxicity of engineered metal oxide nanoparticles. Sci. Total Environ. 407, 3070–3072. https://doi.org/10.1016/j.scitotenv.2009.01.033.

Hu, G., Song, B., Jiang, A., Chu, B., Shen, X., Tang, J., Su, Y., He, Y., 2019. Multifunctional Silicon-Carbon Nanohybrids Simultaneously Featuring Bright Fluorescence, High Antibacterial and Wound Healing Activity. Small 15, 1803200. https://doi.org/10.1002/smll.201803200.

Huang, Z., Dong, P., Zhang, Y., Nie, X., Wang, X., Zhang, X., 2018. A ZIF-8 decorated TiO2 grid-like film with high CO2 adsorption for CO2 photoreduction. J. CO_2 Utilizat. 24, 369–375. https://doi.org/10.1016/j.jcou.2018.01.024.

Ionita, D., Grecu, M., Ungureanu, C., Demetrescu, I., 2011. Antimicrobial activity of the surface coatings on TiAlZr implant biomaterial. J. Biosci. Bioeng. 112, 630–634. https://doi.org/10.1016/j.jbiosc.2011.07.022.

Kao, Y.Y., Chen, Y.C., Cheng, T.J., Chiung, Y.M., Liu, P.S., 2011. Zinc oxide nanoparticles interfere with zinc ion homeostasis to cause cytotoxicity. Toxicol. Sci. 125 (2), 462–472. https://doi.org/10.1093/toxsci/kfr319.

Karlsson, H.L., Toprak, M.S., Fadeel, B., 2014. Toxicity of metal and metal oxide nanoparticle. In: Nordberg, G.F., Fowler, B.A., Nordberg, M. (Eds.), Handbook on the toxicology of metals. fourth ed. Academic Press, London, pp. 75–112.

Liu, Qi, Zhou, Beibei, Miao, Xu., Mao, Guobing, 2017. Integration of nanosized ZIF-8 particles onto mesoporous TiO2 nanobeads for enhanced photocatalytic activity. RSC Adv. 7, 8004. https://doi.org/10.1039/c6ra28277f.

Ma, X., Li, L., Chen, R., Wang, C., Li, H., Li, H., 2018. Highly Nitrogen-Doped Porous Carbon Derived from Zeolitic Imidazolate Framework-8 for CO_2 Capture. Chem. Asian J. 13 (16), 2069–2076. https://doi.org/10.1002/asia.201800548.

Massa, M.A., Covarrubias, C., Bittner, M., Fuentevilla, I.A., Capetillo, P., Von Marttens, A., Carvajal, J.C., 2014. Synthesis of new antibacterial composite coating for titanium based on highly ordered nanoporous silica and silver nanoparticles. Mater. Sci. Eng., C 45, 146–153. https://doi.org/10.1016/j.msec.2014.08.057.

Mohammad, Jalal, Ansari, Mohammad Azam, Ali, Syed Ghazanfar, Khan, Haris M, Rehman, Suriya, 2018. Anticandidal activity of bioinspired ZnO NPs: effect on growth, cell morphology and key virulence attributes of Candida species. Artif. Cells Nanomed. Biotechnol. 1–14. https://doi.org/10.1080/21691401.2018.1439837.

Ordonez, M.J.C., Balkus, K.J., Ferraris, J.P., Musselman, I.H.J., 2010. Molecular sieving realized with ZIF-8/Matrimid® mixed-matrix membranes. J. Membr. Sci. 361 (1–2), 28–37. https://doi.org/10.1016/j.memsci.2010.06.017.

Orooji, Y., Faghih, M., Razmjou, A., Hou, J., Moazzam, P., Emami, N., Aghababaie, M., Nourisfa, F., Chen, V., Jin, W., 2017. Nanostructured mesoporous carbon polyethersulfone composite ultrafiltration membrane with significantly low protein adsorption. Carbon 111, 689–704. https://doi.org/10.1016/j.carbon.2016.10.055.

Orooji, Y., Liang, F., Razmjou, A., Liu, G., Jin, W., 2018. Preparation of anti-adhesion and bacterial destructive polymeric ultrafiltration membranes using modified mesoporous carbon. Sep. Purif. Technol. 205, 273–283. https://doi.org/10.1016/j.seppur.2018.05.006.

Park, K.S., Ni, Z., Côté, A.P., Choi, J.Y., Huang, R., Uribe-Romo, F.J., Chae, H.K., O'Keeffe, M., Yaghi, O.M., 2006. Exceptional chemical and thermal stability of zeolitic imidazolate frameworks. Proc. Natl. Acad. Sci. USA 103 (27), 10186–10191. https://doi.org/10.1073/pnas.0602439103.

Pattengale, B., Yang, S., Lee, S., Huang, J., 2017. Mechanistic probes of zeolitic imidazolate framework for photocatalytic application. ACS Catal. 7 (12), 8446–8453. https://doi.org/10.1021/acscatal.7b02467.

Rasul Rakhshaei, A., Namazi, Hassan, 2017. A potential bioactive wound dressing based on carboxymethyl cellulose/ZnO impregnated MCM-41 nanocomposite hydrogel. Mater. Sci. Eng., C 73, 456–464. https://doi.org/10.1016/j.msec.2016.12.097.

Rath, G., Hussain, T., Chauhan, G., Garg, T., Goyal, A.K., 2016. Development and characterization of cefazolin loaded zinc oxide nanoparticles composite gelatin nanofiber mats for postoperative surgical wounds. Mater. Sci. Eng., C 58, 242–253. https://doi.org/10.1016/j.msec.2015.08.050.

Rehman, S., Asiri, Sarah Mousa, Khan, Firdos Alam, Rabindran Jermy, B., Khan, Hafeezullah, Akhtar, Sultan, Jindan, Reem Al, Khan, Khalid Mohammed, Qurashi, Ahsanulhaq, 2019. Biocompatible Tin Oxide Nanoparticles: Synthesis, Antibacterial, Anticandidal and Cytotoxic Activities. Chem. Select 4, 4013–4017. https://doi.org/10.1002/slct.201803550.

Rehman, S., Jermy, B.R., Akhtar, S., Borgio, J.F., Abdul Azeez, S., Ravinayagam, V., Al Jindan, R., Alsalem, Z.H., Buhameid, A., Gani, A., 2019. Isolation and

characterization of a novel thermophile; Bacillus haynesii, applied for the green synthesis of ZnO nanoparticles. Artif. Cells Nanomed. Biotechnol. 47 (1), 2072–2082. https://doi.org/10.1080/21691401.2019.1620254.

Ren, H., Zhang, L., An, J., Wang, T., Li, L., Si, X., He, L., Wu, X., Wang, C., Su, Z., 2014. Polyacrylic acid@ zeolitic imidazolate framework-8 nanoparticles with ultrahigh drug loading capability for pH-sensitive drug release. Chem. Commun. 50 (8), 1000–1002. https://doi.org/10.1039/C3CC47666A.

Rudramurthy, G.R., Swamy, M.K., Sinniah, U.R., Ghasemzadeh, A., 2016. Nanoparticles: Alternatives Against Drug-Resistant Pathogenic Microbes. Molecules 21, 836. https://doi.org/10.3390/molecules21070836.

Sawai, J., Shoji, S., Igarashi, H., Hashimoto, A., Kokugan, T., Shimizu, M., Kojima, H., 1998. Hydrogen peroxide as an antibacterial factor in zinc oxide powder slurry. J. Ferment. Bioeng. 86, 521–522. https://doi.org/10.1016/S0922-338X(98)80165-7.

Siddiqi, K.S., Rahman, A., Husen, Tajuddin A, 2018. Properties of Zinc Oxide Nanoparticles and Their Activity Against Microbes. Nanosc. Res. Lett. 13, 141. https://doi.org/10.1186/s11671-018-2532-3.

Singh, Madhu, Vander Wal, Randy L., 2019. Nanostructure Quantification of Carbon Blacks C 5, 2. https://doi.org/10.3390/c5010002.

Sirelkhatim, A., Mahmud, S., Seeni, A., Kaus, N.H.M., Ann, L.C., Bakhori, S.K.M., Hasan, H., Mohamad, D., 2015. Review on Zinc Oxide Nanoparticles: Antibacterial Activity and Toxicity Mechanism. Nano-Micro Lett. 7, 219. https://doi.org/10.1007/s40820-015-0040-x.

Song, X., Wang, S., Bao, Y., Liu, G., Sun, W., Ding, L.-X., Liu, H., Wang, H., 2017. A high strength, free-standing cathode constructed by regulating graphitization and the pore structure in nitrogen-doped carbon nanofibers for flexible lithium–sulfur batteries. J. Mater. Chem. A 5, 6832–6839. https://doi.org/10.1039/C7TA01171G.

Sui, M., Zhang, L., Sheng, L., Huang, S., She, L., 2013. Synthesis of ZnO coated multi-walled carbon nanotubes and their antibacterial activities. Sci. Total Environ. 1 (452–453), 148–154. https://doi.org/10.1016/j.scitotenv.2013.02.056.

Thangaraj, R., Senthil Kumar, A., 2012. Graphitized mesoporous carbon modified glassy carbon electrode for selective sensing of xanthine, hypoxanthine and uric acid. Anal. Meth. 4, 2162–2171. https://doi.org/10.1039/C2AY25029B.

Vimbela, G.V., Ngo, S.M., Fraze, C., Yang, L., Stout, D.A., 2017. Antibacterial properties and toxicity from metallic nanomaterials. Int. J. Nanomed. 12, 3941–3965.

Walcarius, A., 2017. Recent Trends on Electrochemical Sensors Based on Ordered Mesoporous Carbon. Sensors 17, 1863. https://doi.org/10.3390/s17081863.

Wang, Y., Cai, R., Chen, C., 2019. The Nano-Bio Interactions of Nanomedicines: Understanding the Biochemical Driving Forces and Redox Reactions. Acc. Chem. Res. 52 (6), 1507–1518. https://doi.org/10.1021/acs.accounts.9b00126.

Wang, J., Wang, Y., Zhang, Y., Uliana, A., Zhu, J., Liu, J., Van der Bruggen, B., 2016. Zeolitic imidazolate framework/graphene oxide hybrid nanosheets functionalized thin film nanocomposite membrane for enhanced antimicrobial performance. ACS Appl. Mater. Interfaces 8 (38), 25508–25519. https://doi.org/10.1021/acsami.6b06992.

Yan, X., Hua, X., Komarnenib, S., 2014. Facile synthesis of mesoporous MOF/silicacomposites. RSC Adv. 4, 57501. https://doi.org/10.1039/c4ra09626f.

Yang, H., Ye, S., Zhou, J., Liang, T., 2019. Biomass-Derived Porous Carbon Materials for Supercapacitor. Front. Chem. 7, 274. https://doi.org/10.3389/fchem.2019.00274.

Yung, M.M.N., Fougères, P.-A., Leung, Y.H., Liu, F., Djurišić, A.B., Giesy, J.P., Leung, K. M.Y., 2017. Physicochemical characteristics and toxicity of surface-modifed zinc oxide nanoparticles to freshwater and marine microalgae. Sci. Rep. 7, 15909. https://doi.org/10.1038/s41598-017-15988-0.

Yusof, H.M., Mohamad, R., Zaidan, U.H., Abdul Rahman, N.A., 2019. Microbial synthesis of zinc oxide nanoparticles and their potential application as an antimicrobial agent and a feed supplement in animal industry: a review. J. Anim. Sci. Biotechnol. 10, 57. https://doi.org/10.1186/s40104-019-0368-z.

Yusuf, K., Badjah-Hadj-Ahmed, A.Y., Aqel, A., AlOthman, Z.A., 2015. Fabrication of zeolitic imidazolate framework-8-methacrylate monolith composite capillary columns for fast gas chromatographic separation of small molecules. J. Chromatogr. A 7 (1406), 299–306. https://doi.org/10.1016/j.chroma.2015.06.026.

Zhang, Yongyong, Jia, Ying, Hou, Li'an, 2018. Synthesis of zeolitic imidazolate framework-8 on polyester fiber for PM2.5 removal. RSC Adv. 8, 31471. https://doi.org/10.1039/c8ra06414h.